

First Principles Computations of the Oxygen Reduction Reaction on Solid Metal Clusters

Cheng-Hung San¹, Chuang-Pin Chiu¹ and Che-Wun Hong^{1,2}

Abstract: An improvement in the catalytic process of oxygen reduction reactions is of prime importance for further progress in low temperature fuel cell performance. This paper intends to investigate this problem from a fundamental quantum mechanics viewpoint. For this purpose, a hybrid density functional theory is employed to analyze the catalytic mechanism of the oxygen reduction at the fuel cell cathode. Major steps in the oxygen reduction that include the oxygen adsorption on solid metal clusters (e.g. Cu and Pt) and complete four proton transfer steps are simulated. Proton transfer processes from hydroniums to the adsorbed oxygen molecules to produce water are observed to be mainly influenced by the electronic cloud at the catalyst. The first principles computation results reveal a difficulty in choosing the catalyst material and how the catalytic mechanism limits the performance of current low temperature fuel cells.

Keywords: Oxygen reduction reaction, Density functional theory, Quantum mechanics, Catalyst

1 Introduction

The oxygen reduction reaction (ORR) mechanism at the cathode of low temperature fuel cells has been a major research topic in the improvement of the power conversion efficiency. The slow rate of the ORR is a major influencing factor that causes a higher over-potential leading to a reduction of the electrochemical performance. Improving the catalytic efficiency is an effective method of increasing ORR rates; an initiative also pursued in proton exchange membrane fuel cells and in most biofuel cells. In the past decade, experimental investigations for understanding the ORR kinetics on various catalysts have been carried out [Collman, Fu, Herrmann,

¹ Department of Power Mechanical Engineering, National Tsing Hua University, Hsinchu 30013, Taiwan

² Corresponding author. Phone: +886-3-5742591; Fax: +886-3-5722840; E-mail: cwhong@pme.nthu.edu.tw

and Zhang (1997); Wang (2005); Selvaraju and Ramaraj (2005); Jiang and Brisard (2007)] Several models on the mechanism of the oxygen reduction at various metal surfaces were also reported [Inoue, Brankovic, Wang, and Adzic (2002); Antonie and Durand (2000); Anderson and Albu (2000); Brisard, Bertrand, Ross, and Markovic (2000); Paulus, Schmidt, Gasteiger, and Behm (2001)].

These research results indicate that the oxygen reduction could occur through two pathways; one is the two-electron reduction which produces hydrogen peroxide while the other is the direct four-electron reduction that produces water which will be investigated in this research. The chosen pathway depends on how oxygen molecules are adsorbed on the catalytic metal surface.

The oxygen dissociation mechanism on the metal surface is another topic worth researching [Panchenko, Koper, Shubina, Mitchell, and Roduner (2004); Zhang and Anderson (2007)]. These investigations also show that the oxygen reduction to water involves two two-electron transfer steps. The first two-electron step, which involves the reductive cleavage of the O-O bond, is a rate-determining step. Therefore, we can concentrate on the transport phenomena at this step. Platinum (Pt) clusters or its nanoparticles are considered as the most commonly used materials for oxygen reduction [Li and Balbuena (2003); Zhang, Ma, and Mukerjee (2004); Maci, Campina, Herrero, and Feliu (2004); Vukmirovic, Zhang, Sasaki, Nilekar, Uribe, Mavrikakis, and Adzic (2007)]. In order to understand the oxygen reduction and hydrogen oxidation kinetics on Pt clusters [Stamenkovic and Markovic (2001); Komanicky, Menzel, and You (2005)], some researches focused on particular reaction orientations. Nowadays, although Pt is still the best catalyst for the ORR, the search for alternatives to the rare metal is still in progress. In previous study results, the copper particles provided sites for oxygen reduction, which may achieve high rates of mass transport [Colley, Macpherson, and Unwin (2008)]. Yim and Klüner developed a chemical strategy for searching platinum substitutes by investigating the chemical bonding interactions along the ORR path and considered the Pd(111), Ag(111) and Au(111) as potential alternatives for oxygen reduction [Yim and Klüner (2008)]. Molecular dynamics (MD) were employed to analyze the hydronium (H_3O^+) transport phenomena in the proton exchange membrane [Cheng, Chen, and Hong (2008); Chen and Hong (2010)], while other research groups were concerned on the kinetic parameters and the oxygen reduction mechanism inside Nafion[®] [Antoine, Bultel, and Durand (2001); Hwang, Park, Sung, and Lee (2011)]. However, in the above literature survey, none of them considered the hydroniums involved in the ORR. Since hydronium ions cross the proton exchange membrane and arrive at the cathode catalyst, we intend to study the complete four electrons transfer processes beginning from the O_2 reduction to the production of water molecules.

Molecular dynamics and computational quantum mechanics techniques were used to observe the physical phenomena in material sciences [Liu and Shen (2010); San and Hong (2011); Chen and Hong (2011)]. Since all the catalytic mechanisms involve atomic cleavage and adsorption, computational quantum mechanics techniques have to be employed [Hong and Tsai (2010); Hong and Chen (2010)]. In this work, a first-principles calculation using the density functional theory (DFT) was adopted to investigate the mechanisms that occur in the aforementioned ORR pathways. The objectives are to know how an oxygen molecule is adsorbed on the Pt and Cu clusters, why the reductive cleavage of the O-O bond occurs, and the phenomena occurring during the proton transfer on the previously adsorbed oxygen molecule. The detailed proton transfer mechanisms can be observed through the computational technique described in the following sections.

2 Density functional theory (DFT) and adsorption energy

DFT is an alternative approach to solve the Schrödinger equation in computational quantum mechanics. The fundamental concept of the DFT is that there is a relationship between the total electronic energy and the overall electronic density. Instead of performing a feat to solve the full wave functions in multi-electron systems, the methodology of the DFT merely attempts to calculate the total electronic energy and the overall electronic density distribution. A functional enables a function to be mapped to a number and is usually expressed by square brackets as shown below. In the DFT, the energy functional E is a summation of two terms:

$$E[\rho(r)] = \int V_{ext}(r)\rho(r)dr + F[\rho(r)] \quad (1)$$

where \vec{r} is the position vector, $\rho(\vec{r})$ is the density function. The first term at the right hand side represents the electron interactions with an external potential $V_{ext}(\vec{r})$. The second term, $F[\rho(\vec{r})]$, is the sum of the kinetic energy of the electrons and the contribution from inter-electronic interactions. The above equation is the DFT equivalent of the Schrödinger equation. From the work of Kohn and Sham [Kohn and Sham (1965)], the approximate functional E can be partitioned into four terms as shown below:

$$E[\rho(r)] = E_T[\rho(r)] + E_V[\rho(r)] + E_J[\rho(r)] + E_{XC}[\rho(r)] \quad (2)$$

where E_T is the kinetic energy term resulting from electron motion; E_V includes terms describing the potential energy of the nuclear-electron attraction and the repulsion between pairs of nuclei; E_J is the electron-electron repulsion term; and E_{XC} represents the exchange-correlation term which includes the remaining part of

the electron-electron interactions. All terms are functions of the electron density function $\rho(\vec{r})$, except for the nuclear-nuclear repulsion. In this simulation, a well-tested B3LYP was adopted, which pairs with Becke's gradient-corrected exchange functional with the gradient-corrected correlation functional of Lee, Yang and Parr [Lee, Yang, and Parr (1988)]. This hybrid exchange-correlation functional, E_{XC}^{B3LYP} , is expressed by:

$$E_{XC}^{B3LYP} = E_{XC}^{LDA} + a_0(E_X^{HF} - E_X^{LDA}) + a_x(E_X^{CGA} - E_X^{LDA}) + a_c(E_X^{CGA} - E_X^{LDA}) \quad (3)$$

where E_{XC}^{LDA} is the local-density approximation (LDA) to the exchange-correlation functional; E_X^{HF} is the Hartree-Fock exact exchange functional; E_X^{CGA} and E_C^{CGA} are generalized gradient approximations (GGA) of the exchange functional and the correlation functional, respectively. The three weighting coefficients are input as $a_0 = 0.20, a_x = 0.72$, and $a_c = 0.80$.

The second approximation is the molecular orbital expression, which is represented by a linear combination of a pre-defined set of single-electron functions known as the basis functions. The Gaussian09 code [Frisch et al. (2009)], which adopts Gaussian-type atomic functions as basis functions, was used for this purpose. The general form is:

$$G(\alpha, \vec{r}) = c \cdot x^n y^m z^l e^{(-\alpha \cdot r^2)} \quad (4)$$

where α is a constant determining the size (radial extent) of the function; \vec{r} is the position vector which is composed of the x, y and z positions; n, m and l are the principal, magnetic and azimuthal quantum numbers, respectively; c is a coefficient depending on the quantum numbers. 6-31G basis set was chosen for O, H and Cu atoms, while another LanL2DZ basis set was used for the Pt atoms.

The adsorption energy of molecules on the slab surface is calculated from the energy balance:

$$E_{ads} = E_{slab} + E_{molecule} - E_{(slab+molecule)} \quad (5)$$

where E_{slab} is the energy of the slab; $E_{molecule}$ is the specific molecular energy; $E_{(slab+molecule)}$ is the total energy of the adsorbed molecules on the slab surface. A positive value of the adsorption energy calculated from the above equation indicates a stable adsorption; the greater the more stable.

3 Results and analyses

3.1 Oxygen adsorption on the metal clusters

Oxygen adsorption on the metal surface is regarded as the first step in the oxygen reduction mechanism. Geometry optimizations of the oxygen adsorption on the

Cu₂ (2 Cu atoms) and Pt₂ (2 Pt atoms) are determined by using the DFT computation. In Fig. 1(a) and Fig. 1(b), the left hand side is the initial molecular structure and the right hand side shows the stable adsorption structure of oxygen molecules with the Cu and Pt atoms, respectively. The bond lengths between the Cu-O and Pt-O pairs are 1.73 Å, and 1.93 Å, respectively. The values are an indication that the bond strength between the Cu-O pair is stronger than the Pt-O bond. Clearly, the original O-O bond is stretched to a longer distance when the oxygen molecules are adsorbed on the Pt₂ or Cu₂ atoms. In addition, both the Cu-O and Pt-O bonds are strong enough to break up the double bond between the original oxygen atoms. The bond angles between the O-Cu-Cu and the O-Pt-Pt are evaluated to be 79.3 and 74.3, respectively; the bond length between the O-O pair after the adsorption with the Cu atoms is 1.65 Å and 1.53 Å for the case of the adsorption on the Pt atoms. It is concluded that the strength of the O-O bond after the adsorption with the Cu atoms is weaker than the case with the Pt atoms. This implies that the Cu atoms are a more effective catalyst than Pt atoms in the O₂ adsorption and O-O bond cleavage at this stage.

The next case is to study a more realistic oxygen adsorption condition by using several clusters such as: Cu₉ (9 Cu atoms), Pt₉ (9 Pt atoms), Cu₁₈ (18 Cu atoms), and Pt₁₈ (18 Pt atoms). Figure 2 shows the optimized geometry of the adsorbed oxygen molecules for the above cases. All the detailed results of the optimized adsorption geometry are summarized in Table 1. The bond length of the Cu-O pair is 1.86 Å on the Cu₉ cluster (100) surface and 1.91 Å on the Cu₁₈ cluster (100) surface. The O-O bond length is 1.61 Å on the Cu₉ surface and 1.63 Å on the Cu₁₈ surface. On the cases of the Pt₉ and the Pt₁₈ surfaces, the Pt-O bond lengths are 2.06 Å and 2.05 Å, respectively; the O-O bond lengths are 1.40 Å and 1.48 Å, respectively. The adsorption energy of oxygen molecules is greater on the Cu₉ (100) surface (55.72 kCal-mole⁻¹) than on Cu₁₈ (100) surface (54.59 kCal-mole⁻¹). The difference of the oxygen adsorption energy between two cases, Cu₉ and Cu₁₈, is small and the optimized geometry of oxygen adsorbed structure is also similar. As shown in Fig. 2, those two oxygen atoms are stretched to a distance of 1.63 Å on the Cu₁₈ surface and 1.61 Å on the Cu₉ surface. Similar phenomena can also be found in the adsorption on Pt₉ and Pt₁₈ surfaces. The distance between two oxygen atoms is larger on the Pt₁₈ surface (1.48 Å) than on the Pt₉ surface (1.40 Å). Hence, the oxygen molecule adsorption on the Pt₁₈ cluster surface has larger positive adsorption energy (53.72 kCal-mole⁻¹) than that of the Pt₉ surface (38.54 kCal-mole⁻¹). By comparing the adsorption energy and the O-O bond length on the Cu surface with that on the Pt surface, two conclusions are at hand. First, the oxygen adsorption on the Cu cluster surface is more stable than on the Pt cluster surface (from 55.72 kCal-mole⁻¹ to 38.54 kCal-mole⁻¹ and

from 54.59 kCal-mole⁻¹ to 53.72 kCal-mole⁻¹). Second, the O-O bond in the oxygen molecule can be more easily cleaved on the Cu surface than on the Pt cluster surface depending on their bond lengths (from 1.61 Å to 1.40 Å (Cu) and from 1.63 Å to 1.48 Å (Pt)).

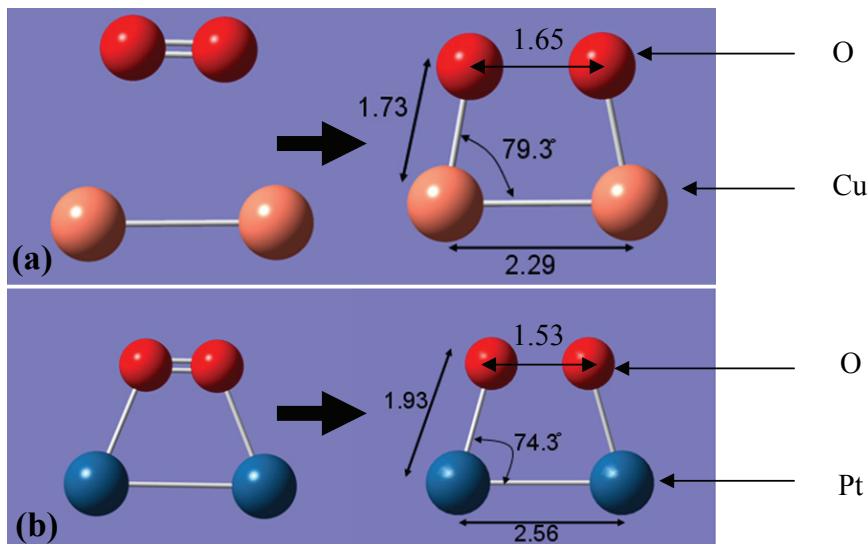


Figure 1: The optimized structure of the oxygen adsorption with (a) two Cu atoms and (b) two Pt atoms, respectively. The unit of the bond length is Å.

Table 1: Adsorption energies and associated bond distances for oxygen molecules adsorbed on the surface of Cu and Pt clusters

Case	O-Metal	O-O	Adsorption energy
Cu_9 (100)	1.86 Å	1.61 Å	55.72 kCal-mole ⁻¹
Pt_9 (100)	2.06 Å	1.40 Å	38.54 kCal-mole ⁻¹
Cu_18 (100)	1.91 Å	1.63 Å	54.59 kCal-mole ⁻¹
Pt_18 (100)	2.05 Å	1.48 Å	53.72 kCal-mole ⁻¹

Figure 3 shows the process of how the oxygen molecule is adsorbed and cleaved on two Cu atoms according to the scan of the total energy variation. As shown in this

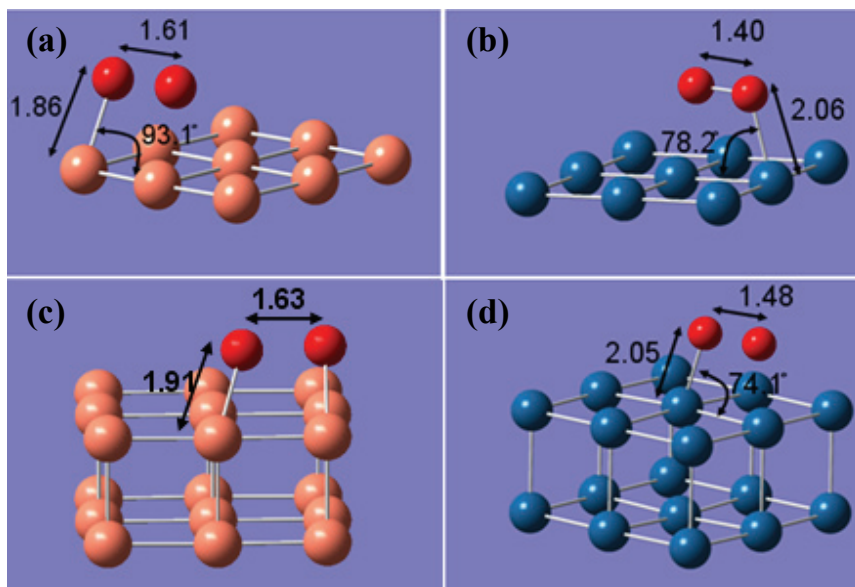


Figure 2: The optimized geometry of the oxygen adsorption on the (a) Cu₉(100), (b) Pt₉(100), (c) Cu₁₈(100) and (d) Pt₁₈(100) cluster surface.

figure, the total energy has the highest value before the oxygen molecular adsorption. When the oxygen atoms bind to the Cu atoms, the bond between the oxygen atoms starts to cleave until these two oxygen atoms are separated to a distance of 1.65 Å. The lowest energy location represents the most stable oxygen adsorption energy. On the other hand, Figure 4 shows the scan of the total energy variation due to the adsorption and cleavage of the oxygen molecule on two Pt atoms. As expected, the total energy of the system has its highest value before the oxygen adsorption. The lowest energy point represents the most stable structure after the oxygen adsorption on the two Pt atoms. However, when the two oxygen atoms stretch further from the most stable structure, the total energy rises again until the separation distance reaches 2.12 Å, at which point it begins to decrease with an increasing scan distance. However, the relation between the total energy and the scan coordinate is not so stable, because the number of Pt atoms involved in the calculation is not large enough. Figure 5 represents the stabilized condition for Pt₁₈ and Cu₁₈ clusters. In both cases, it can be seen that the total energy is monotonously

decreased when both oxygen atoms are adsorbed on the much larger Pt₁₈ cluster. The oxygen molecule approaches the catalyst surface with different angles when the actual oxygen adsorption process takes place. Essentially, the angle of incidence in which that the oxygen molecule approaches the catalyst should have an effect on the adsorption process. To test this hypothesis, three approaching (orientation) angles are considered in the computation. Figure 6 shows the adsorbed oxygen molecule on the Pt₁₈ cluster with different orientation angles; 0°, 45°, 90°, respectively. The left side of each sub-figure is an un-optimized oxygen adsorption structure, while the right hand side shows its optimized counterpart. Using a geometrical analysis, the optimized structure is almost the same in all three computed cases. The O-Pt length is 2.05Å and the distance between the two oxygen atoms is stretched to a final length of 1.48Å in all three cases. Table 2 shows a comprehensive collection containing adsorption energies (all are around 53.70kCal-mol⁻¹) and geometric data of the optimized structure after oxygen molecules are adsorbed on the Pt₁₈ cluster with different orientation angles. A similar case was studied on the adsorbed oxygen molecule on the Cu cluster with different orientation angles (0°, 45°, 90°) and shown in Fig. 7. Table 3 shows that the O-Cu bond lengths, O-O bond lengths, and adsorption energies are 1.91Å, 1.63Å, and 54.59 kCal-mole⁻¹, respectively, in the different orientation conditions.

Table 2: Adsorption energies and geometric data of the optimized structure after oxygen molecules are adsorbed on the Pt₁₈ cluster from different orientation angles

Orientation	O-Pt length	O-O length	Adsorption energy
0°	2.05	1.48	53.72 kCal-mole ⁻¹
45°	2.05	1.48	53.69 kCal-mole ⁻¹
90°	2.05	1.48	53.69 kCal-mole ⁻¹

Table 3: Adsorption energies and the geometry data of the optimized structure after oxygen molecules are adsorbed on the Cu₁₈ cluster from different orientation angles

Orientation	O-Cu length	O-O length	Adsorption energy
0°	1.91	1.63	54.59 kCal-mole ⁻¹
45°	1.91	1.63	54.59 kCal-mole ⁻¹
90°	1.91	1.63	54.59 kCal-mole ⁻¹

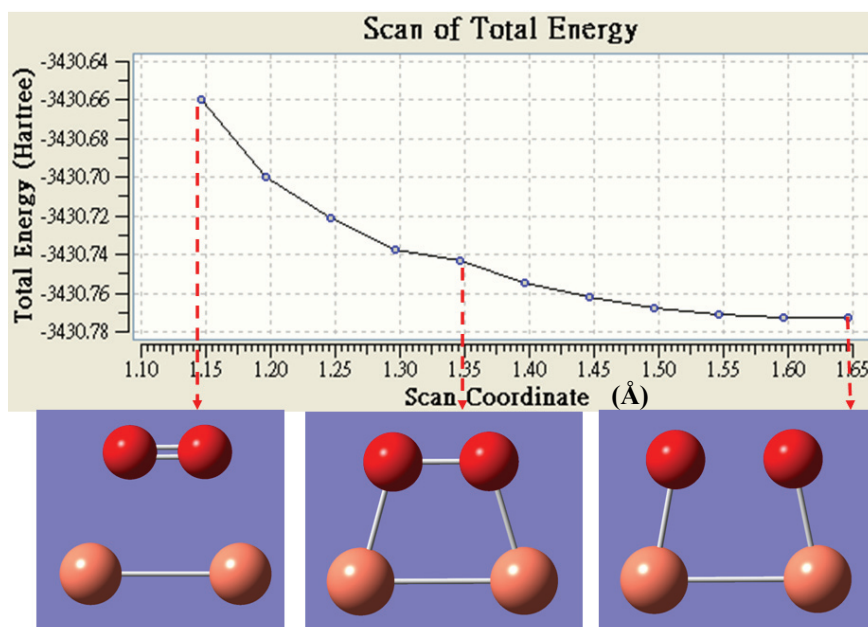


Figure 3: The process of how the oxygen molecule is adsorbed and cleaved on two Cu atoms according to the scan of the total energy variation.

3.2 Hydroniums involved in the ORR

A further investigation on the proton transfer mechanism is now presented in detail. Since hydronium ions (H_3O^+) cross the proton exchange membrane and arrive at the cathode catalyst, we intend to study the complete reaction from the O_2 reduction to the production of water molecules step by step. The desired reaction is the four-electron reduction to water which is expressed as below:



The DFT calculation on the adsorption of the first hydronium on two metal cluster models (Pt₁₈ and Cu₁₈) is performed and shown in Fig. 8. When one of the three hydrogen protons in the hydronium ion starts to bind with one of the oxygen atoms in the oxygen molecule, a cleavage between the Pt-O bond takes place with a newly formed hydroxyl radical (OH^-), as shown at the right hand side in Fig. 8(a). In the case of the Cu₁₈ surface (see Fig. 8(b)), the proton is also transferred from the hydronium to the adsorbed oxygen atom forming a hydroxyl radical. The

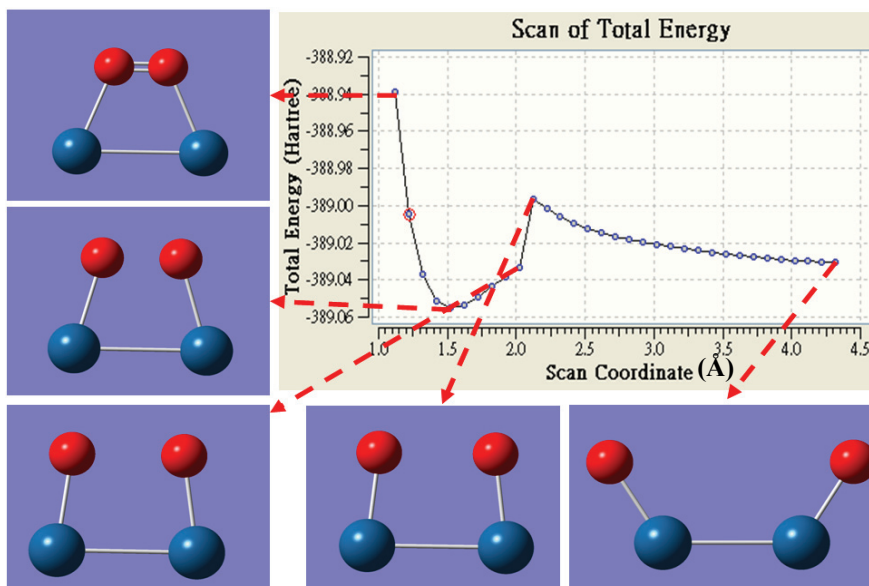


Figure 4: The scan of the total energy variation due to the adsorption and cleavage of the oxygen molecule on two Pt atoms.

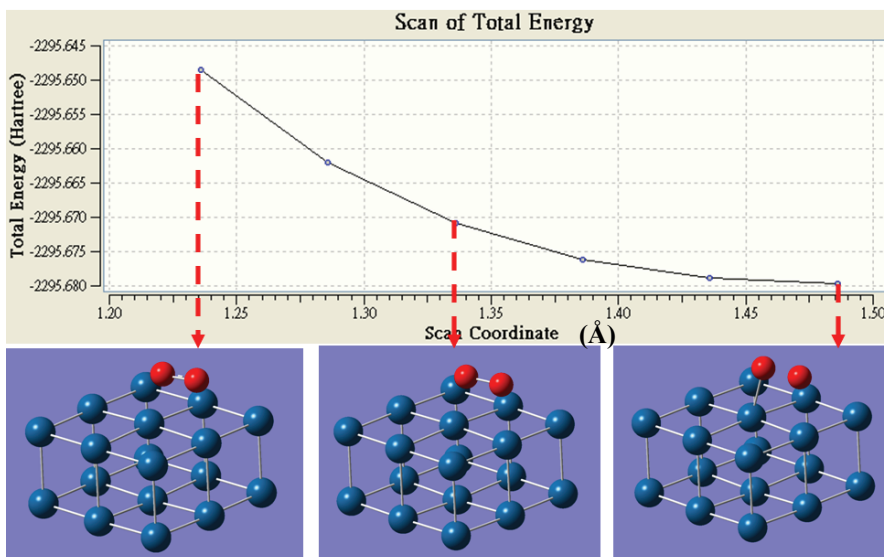


Figure 5: The scan of the total energy variation due to the adsorption and cleavage of the oxygen molecule on the Pt₁₈ cluster.

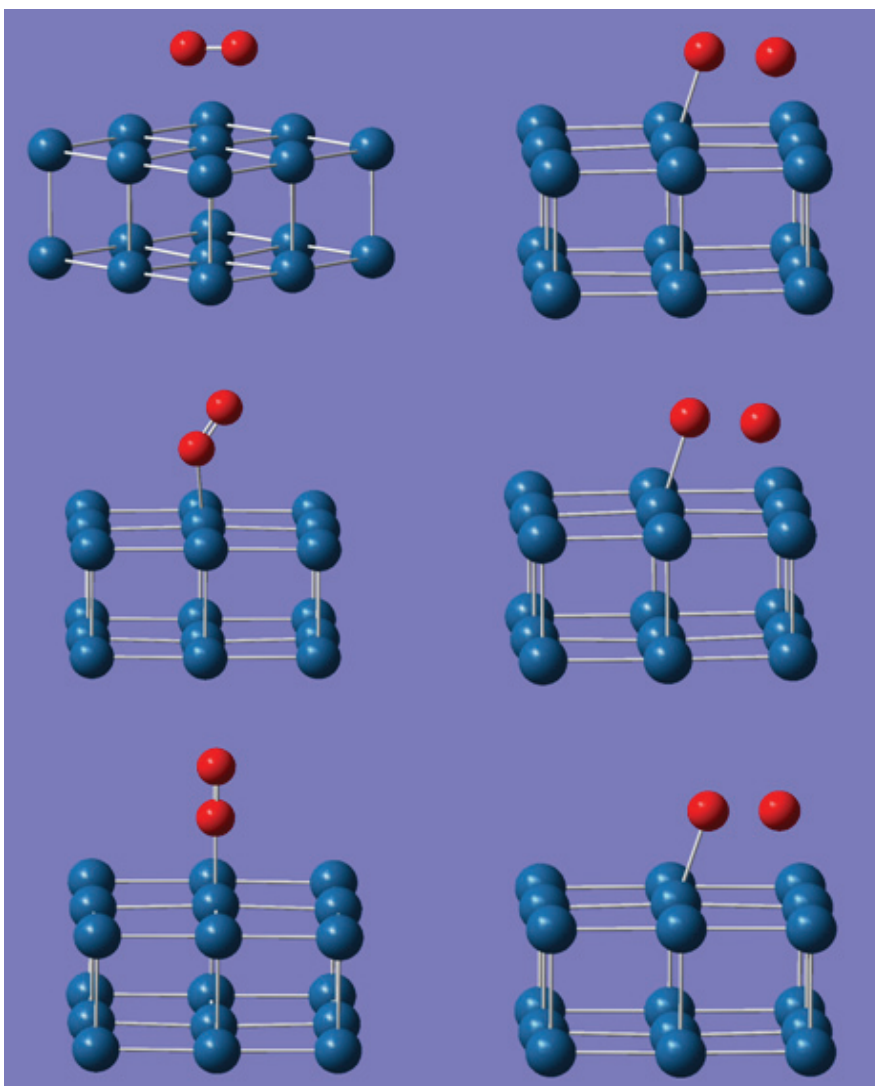


Figure 6: Oxygen molecule is adsorbed on Pt₁₈ cluster with different orientation angles; (a) 0°, (b) 45° and (c) 90°, respectively.

parameter which determines whether the hydroxyl radical is able to move away from the catalyst surface or not depends on the distance between the metal and the O-H radical. The farther the distance is, the greater the chance for the hydroxyl to move away. Figure 8(a) shows that the Pt-O bond length stretches from 2.05Å to 2.50Å; and similarly Cu-O bond length stretches from 1.93Å to 2.08Å in Fig. 8(b).

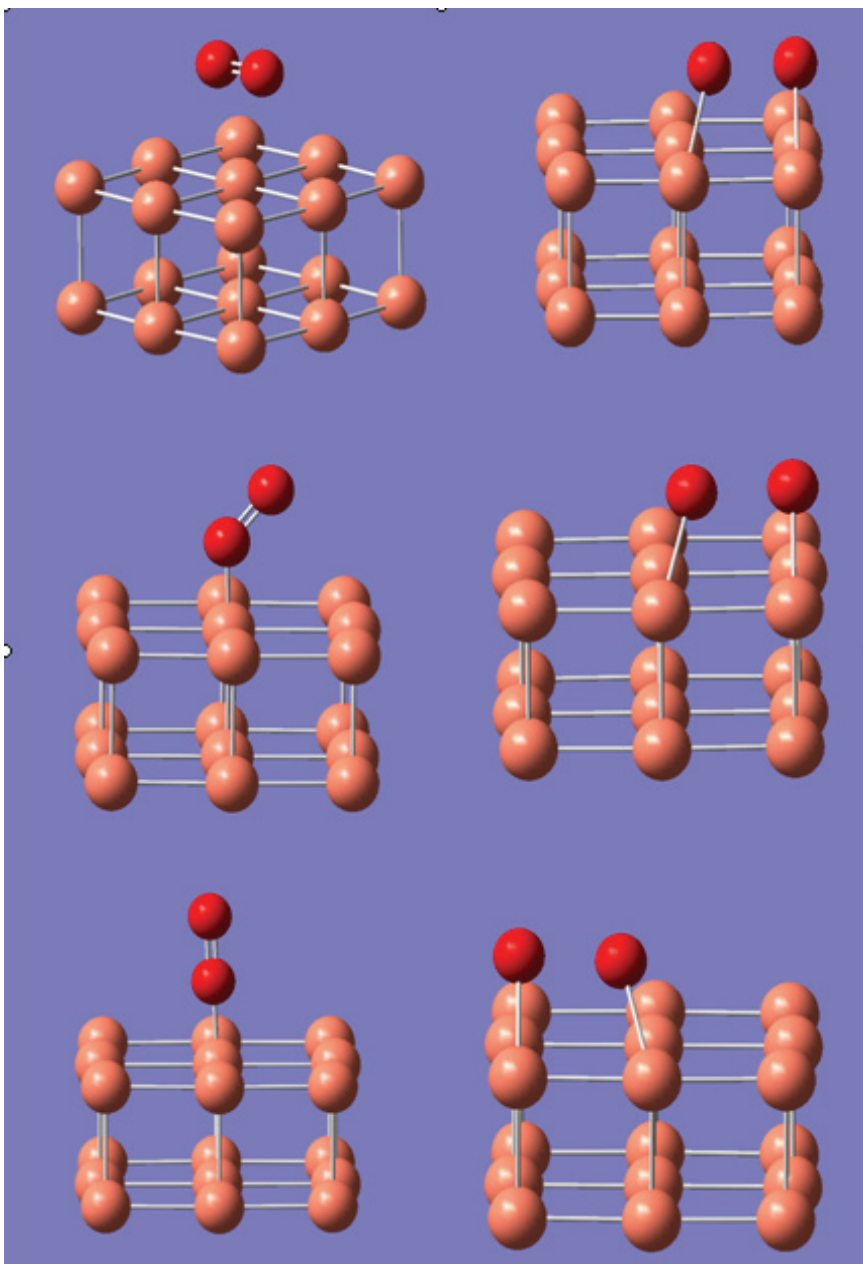


Figure 7: Oxygen molecule is adsorbed on Cu₁₈ cluster with different orientation angles; (a) 0°, (b) 45° and (c) 90°, respectively.

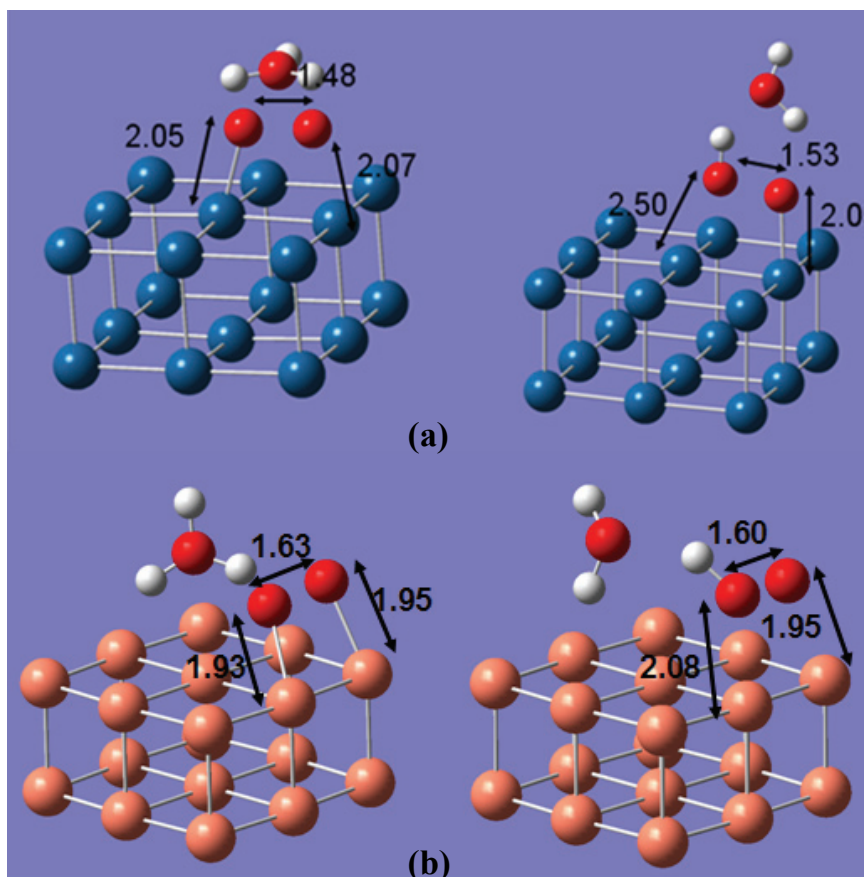


Figure 8: The proton transfer process of the first hydronium ion approaches (a) the O₂ adsorbed Pt₁₈ cluster and (b) the O₂ adsorbed Cu₁₈ cluster. A hydroxyl radical is formed in both cases and the bond length between the OH⁻ and the metal surface all stretches to a longer distance.

Therefore, it is now possible for another oxygen atom, which is not bound to the proton, to come into action and force the hydroxyl radical to move away from the catalyst surface.

The subsequent 2nd, 3rd, and 4th hydronium ions that approach the O₂ adsorbed Pt₁₈ and Cu₁₈ surfaces are shown in Fig. 9 and Fig. 10, respectively. Figure 9(a) displays the following steps after the first hydronium molecule has entered and reacted with the oxygen atom to produce OH⁻. At this time, the OH⁻ radical leaves

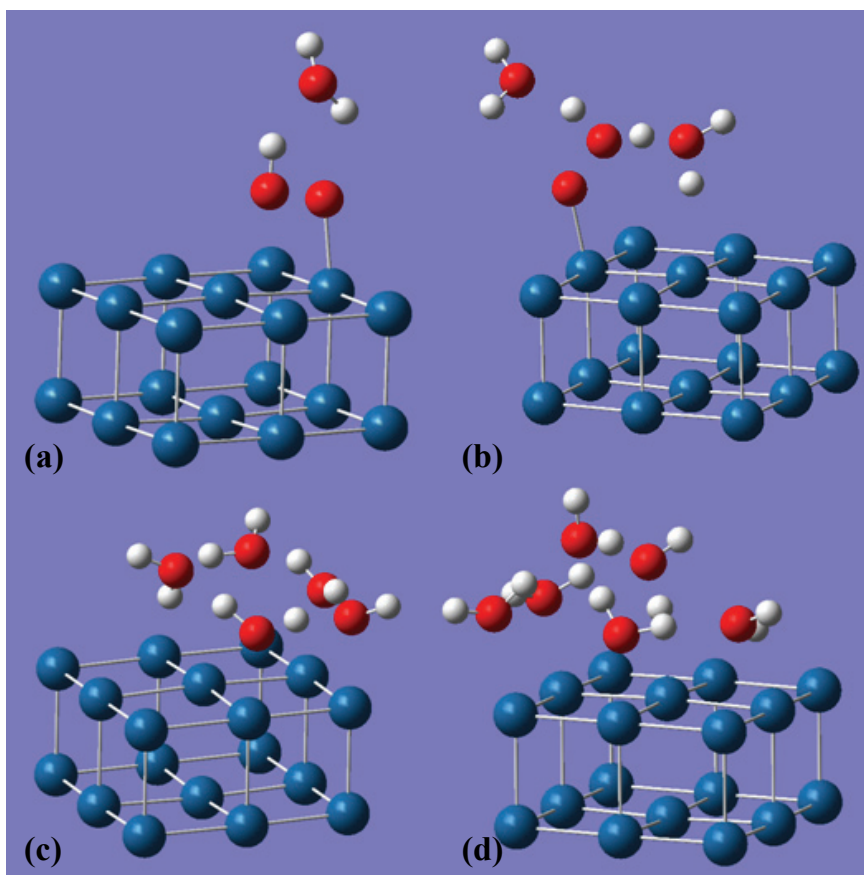


Figure 9: The stabilized molecular structures of (a) the 1st and subsequently (b) the 2nd, (c) the 3rd, and (d) the 4th hydronium ions approach the O₂ adsorbed Pt₁₈ surface. The last one shows that six water molecules are generated and complete the oxygen reduction reaction.

the Pt surface. It is noted that an O atom is presently adsorbed on the Pt surface. In the next step, shown in Fig. 9(b), the second hydronium ion enters and separates into three H protons and one O atom. At this point, the bond between the Pt surface and the single O atom still exists. Afterwards, as the third hydronium arrives, the O adsorbed on the Pt surface reacts and departs from the catalyst surface to become OH⁻, as shown in Fig. 9(c). In the last ORR mechanism, a fourth hydronium molecule enters (see Fig. 9(d)) causing the OH⁻ radical to react and form six H₂O

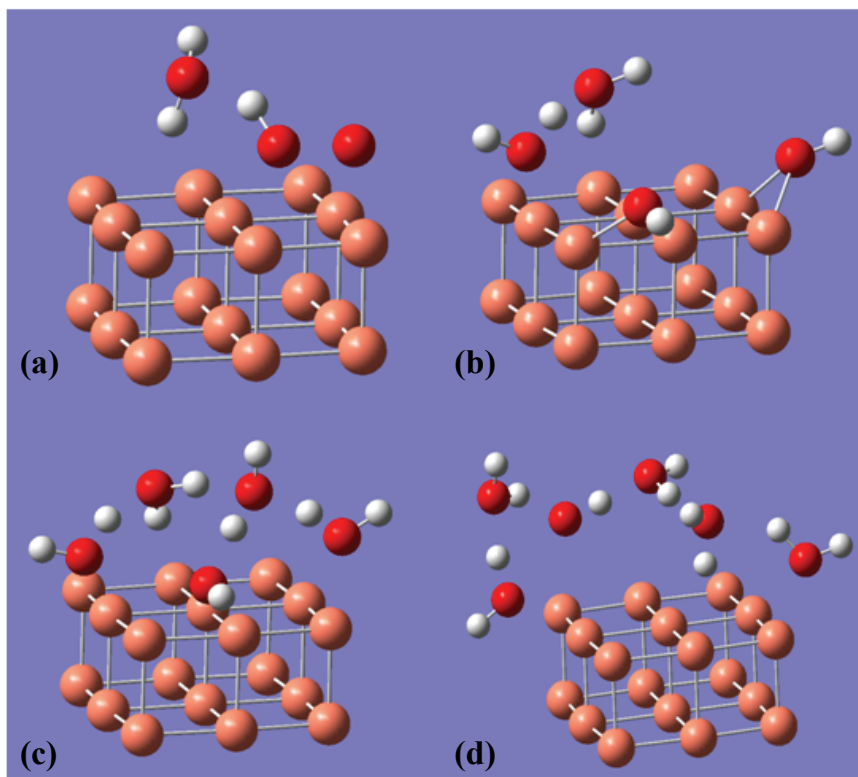


Figure 10: The stabilized molecular structures of (a) the 1st and subsequently (b) the 2nd, (c) the 3rd, and (d) the 4th hydronium ions approach the O₂ adsorbed Cu₁₈ surface. The last one shows that six water molecules are generated and complete the oxygen reduction reaction. Note that one of the hydrogen protons is shaded by an oxygen atom.

molecules to complete the oxygen reduction reaction written in Eq. (6). Similarly, the ORR process described for the Pt surface can be applied to the Cu surface (see Fig. 10(a) to Fig. 10(d)).

For a more comprehensive comparison of the ORR mechanism between Pt₁₈ and Cu₁₈ surfaces, we summarize the total energies and energy differences at the six steps of the ORR process described above (refer to Table 4). Step 1 to step 6, as shown in Fig. 11(a), represent the initial condition, the oxygen adsorption on the catalyst surface, the first hydronium involvement, the second hydronium entrance, the approach of the third hydronium, and the arrival of the fourth hydronium, re-

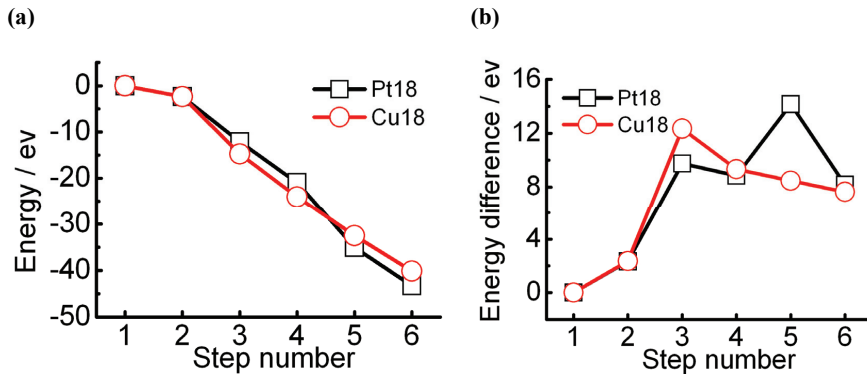


Figure 11: (a) The total energies and (b) the energy differences at the six steps of the ORR process described in the text. Step 1 to step 6 represent the initial condition, the oxygen adsorption on the catalyst surface, the first hydronium involvement, the second hydronium entrance, the approach of the third hydronium, and the arrival of the fourth hydronium, respectively.

spectively. The energy difference value between each step is proportional to the reaction rate at this step for the ORR. In the Pt case, the highest reaction rate occurs at the arrival of the third hydronium molecule, as shown in Fig 11(b). However, in the Cu case, the fastest ORR reaction rate takes place when the first hydronium is involved.

4 Conclusion

In most low temperature fuel cells, the ORR mechanism at the cathode plays the key role to limit the reaction rate of the fuel cell, and thus the performance. The quantum simulation results in this research indicate that: (a) the Cu surface is more beneficial to the oxygen adsorption than the Pt surface; (b) the O-O bond within the oxygen molecule is broken more easily on the Cu cluster surface than on the Pt surface; (c) a hydroxyl radical can be formed on the catalyst surface when the first hydronium comes near the oxygen adsorbed cluster; (d) the hydroxyl radical departs from the Pt cluster surface more easily than from the Cu cluster; (e) in the Pt_18 case, the highest reaction rate occurs at the arrival of the third hydronium ion (step 5). However, in the Cu_18 case, the fastest ORR rate takes place when the first hydronium is involved (step 3).

Based on the present model study, it can be concluded that the O₂ adsorption is

Table 4: Calculation of the total energy at each step and the energy difference between each step of the O₂ reduction at Pt₁₈ and Cu₁₈ clusters. The bold letters indicate that the step at which the highest reaction rate may take place.

	Total energy (and difference) on the Pt ₁₈ cluster	E_{Pt} (eV)	ΔE_{Pt} (eV)
Step 1	E[O ₂]	0	0
Step 2	E[Pt ₁₈ +O ₂]-E[Pt ₁₈]-E[O ₂]	-2.33	2.33
Step 3	E[Pt ₁₈ +O ₂ +1H ₃ O ⁺]-E[Pt ₁₈]-E[O ₂]-1E[H ₃ O ⁺]	-12.08	9.75
Step 4	E[Pt ₁₈ +O ₂ +2H ₃ O ⁺]-E[Pt ₁₈]-E[O ₂]-2E[H ₃ O ⁺]	-20.92	8.84
Step 5	E[Pt ₁₈ +O ₂ +3H ₃ O ⁺]-E[Pt ₁₈]-E[O ₂]-3E[H ₃ O ⁺]	-35.08	14.16
Step 6	E[Pt ₁₈ +O ₂ +4H ₃ O ⁺]-E[Pt ₁₈]-E[O ₂]-4E[H ₃ O ⁺]	-43.25	8.17
	Total energy (and difference) on the Cu ₁₈ cluster	E_{Cu} (eV)	ΔE_{Cu} (eV)
Step 1	E[O ₂]	0	0
Step 2	E[Cu ₁₈ +O ₂]-E[Cu ₁₈]-E[O ₂]	-2.37	2.37
Step 3	E[Cu ₁₈ +O ₂ +1H ₃ O ⁺]-E[Cu ₁₈]-E[O ₂]-1E[H ₃ O ⁺]	-14.71	12.34
Step 4	E[Cu ₁₈ +O ₂ +2H ₃ O ⁺]-E[Cu ₁₈]-E[O ₂]-2E[H ₃ O ⁺]	-24.05	9.34
Step 5	E[Cu ₁₈ +O ₂ +3H ₃ O ⁺]-E[Cu ₁₈]-E[O ₂]-3E[H ₃ O ⁺]	-32.51	8.46
Step 6	E[Cu ₁₈ +O ₂ +4H ₃ O ⁺]-E[Cu ₁₈]-E[O ₂]-4E[H ₃ O ⁺]	-40.16	7.65

the slowest step in the ORR mechanism. The highest reaction rate may occur at the arrival of the third hydronium ion (step 5) on the Pt cluster, and at the first hydronium arrival on the Cu cluster. Once the four-electron reduction is complete, the final product contains six water molecules. They can be displaced by incoming oxygen molecules, so that the ORR cycle can be repeated. Our work has identified the pathway of the ORR process in hydrogen fuel cells, further experimental verification is necessary.

Acknowledgement: Thanks are due to the National Science Council of Taiwan and the Tsing Hua Boost Program which supported this research under the grant numbers: NSC 98-2221-E-007-108-MY3 and NTHU99N2521E1. We are also grateful to the National Center for High-Performance Computing for the generous computer time and facilities.

References

- Anderson A.B.; Albu T.V.** (2000): Catalytic effect of platinum on oxygen reduction an ab initio model including electrode potential dependence, *J. Electrochem. Soc.*, vol. 147, pp. 4229-4238.
- Antonie O.; Durand R.** (2000): RRDE study of oxygen reduction on Pt nanoparti-

cles inside Nafion: H₂O₂ production in PEMFC cathode conditions, *J. Appl. Electrochem.*, vol. 30, pp. 839-844.

Antoine O.; Bultel Y.; Durand R. (2001): Oxygen reduction reaction kinetics and mechanism on platinum nanoparticles inside Nafion, *J. Electroanal. Chem.*, vol. 499, pp. 85-94.

Brisard G.; Bertrand N.; Ross P.N.; Markovic N.M. (2000): Oxygen reduction and hydrogen evolution–oxidation reactions on Cu(hkl) surfaces, *J. Electroanal. Chem.*, vol. 480, pp. 219-224.

Chen P.Y.; Hong C.W. (2010): Nanoscale transport dynamics inside a hydrated Nafion membrane with electric field effects, *Fuel Cells*, vol. 10, pp.17-25.

Chen W.H.; Hong C.W. (2011): Nano-array solid electrode design for photoelectrochemical solar cells, *CMC: computers materials & continua*, vol.21, pp.147-170.

Cheng C.H.; Chen P.Y.; Hong C.W. (2008): Atomistic analysis of hydration and thermal effects on proton dynamics in the Nafion membrane, *J. Electrochem. Soc.*, vol. 155, pp. 435-442.

Colley A.L.; Macpherson J.V.; Unwin P.R. (2008): Effect of high rates of mass transport on oxygen reduction at copper electrodes: Implications for aluminium corrosion, *Electrochem. Commun.*, vol. 10, pp. 1334-1336.

Collman J.P.; Fu L.; Herrmann P.C.; Zhang X. (1997): A functional model related to Cytochrome c oxidase and its electrocatalytic four-electron reduction of O₂, *Science*, vol. 275, pp. 949-951.

Frisch M.J. et al. (2009): *Gaussian 09 Revision A1 Gaussian Inc.*, Wallingford CT.

Hong C.W.; Tsai C.Y. (2010): Computational quantum mechanics simulation on the photonic properties of group-III Nitride clusters, *CMES: Computer Modeling in Engineering & Sciences*, vol.67, pp.79-94.

Hong C.W.; Chen W.H. (2011): Computational quantum chemistry on the photoelectric characteristics of semiconductor quantum dots and biological pigments, *CMES: Computer Modeling in Engineering & Sciences*, vol.72, pp.211-228.

Hwang D.S.; Park C.H.; Sung C.; Lee Y.M. (2011): Optimal catalyst layer structure of polymer electrolyte membrane fuel cell, *Int. J. Hydrogen. Energ.*, vol. 36, pp. 9876-9885.

Inoue H.; Brankovic S.R.; Wang J.X.; Adzic R.R. (2002): Oxygen reduction on bare and Pt monolayer-modified Ru(0001), Ru(1010) and Ru nanostructured surfaces, *Electrochim. Acta*, vol. 47, pp. 3777-3785.

Jiang T.; Brisard G.M. (2007): Determination of the kinetic parameters of oxygen

reduction on copper using a rotating ring single crystal disk assembly (RRD_{Cu(hkl)}E), *Electrochim. Acta*, vol. 52, pp. 4487–4496.

Kohn W.; Sham L.J. (1965): Self-consistent equations including exchange and correlation effects, *Phys. Rev.*, vol. 140, pp.1133-1138.

Komanicky V.; Menzel A.; You H. (2005): Investigation of oxygen reduction reaction kinetics at (111)-(100) nanofaceted platinum surfaces in acidic media, *J. Phys. Chem. B*, vol. 109 pp. 23550-23557.

Li T.; Balbuena P.B. (2003): Oxygen reduction on a platinum cluster, *Chem. Phys. Lett.*, vol. 367, pp.439-447.

Lee C.; Yang W.; Parr R.G. (1988): Development of the Colic-Salvetti correlation-energy formula into a functional of the electron density, *Phys. Rev. B*, vol. 37, pp. 785-789.

Liu Q.; Shen S. (2010): Effects of surface orientation and temperature on tensile deformation of gold nanowires, *CMC: computers materials & continua*, vol.17, pp.59-75.

Maci M.D.; Campina J.M.; Herrero E.; Feliu J.M. (2004): On the kinetics of oxygen reduction on platinum stepped surfaces in acidic media, *J. Electroanal. Chem.*, vol. 564, pp. 141-150.

Panchenko A.; Koper A.T.M.; Shubina T.E.; Mitchell S.J.; Roduner E. (2004): Ab initio calculations of intermediates of oxygen reduction on low-index platinum surfaces, *J. Electrochem. Soc.*, vol. 151, pp. 2016-2027.

Paulus U.A.; Schmidt T.J.; Gasteiger H.A.; Behm R.J. (2001): Oxygen reduction on a high-surface area Pt/Vulcan carbon catalyst: a thin-film rotating ring-disk electrode study, *J. Electroanal. Chem.*, vol. 495, pp.134-145.

San C.H.; Hong C.W. (2011): Molecular design of the solid copolymer electrolyte-poly (styrene-b-ethylene oxide) for lithium ion batteries, *CMC: computers materials & continua*, vol.23, pp.101-117.

Selvaraju T.; Ramaraj R (2005): Nanostructured copper particles-incorporated Nafion- modified electrode for oxygen reduction, *Praman-J. Phys.*, vol. 65, pp. 713-722.

Stamenkovic V.; Markovic N.M. (2001): Oxygen reduction and hydrogen oxidation reactions on Pt(111) and Pt(100) in solutions containing copper ions, *Langmuir*, vol. 17, pp. 2388-2394.

Vukmirovic M.B.; Zhang J.; Sasaki K.; Nilekar A.U.; Uribe F.; Mavrikakis M.; Adzic R.R. (2007): Platinum monolayer electrocatalysts for oxygen reduction, *Electrochim. Acta*, vol. 52, pp. 2257-2263.

Wang B. (2005): Recent development of non-platinum catalysts for oxygen reduc-

tion reaction, *J. Power Sources*, vol. 152, pp.1-15.

Yim W.L.; Klüner T. (2008): Promoting O₂ activation on noble metal surfaces, *J. Catal.*, vol. 254, pp. 349-354.

Zhang L.; Ma C.; Mukerjee S. J. (2004): Oxygen reduction and transport characteristics at a platinum and alternative proton conducting membrane interface, *Electroanal. Chem.*, vol. 568, pp. 273-291.

Zhang T.; Anderson A.B. (2007): Oxygen reduction on platinum electrodes in base: Theoretical study, *Electrochim. Acta*, vol. 53, pp. 982-989.